HHS Public Access

Author manuscript

Analyst. Author manuscript; available in PMC 2016 February 09.

Published in final edited form as:

Analyst. 2016 February 8; 141(4): 1421–1433. doi:10.1039/c5an02048d.

Amplification-free *In Situ KRAS* Point Mutation Detection at 60 copies/mL in Urine in a Background of 1000-fold Wild Type

Ceyhun E. KirimLi[a], **Wei-Heng Shih**[b], and **Wan Y. Shih**[c]

[a]Drexel University, School of Biomedical Engineering, Science, and Health Systems, Philadelphia, Pennsylvania, USA. ceyhunkirimli@g.harvard.edu

[b]Drexel University, Department of Materials Science and Engineering, Philadelphia, Pennsylvania, USA

[c]Drexel University, School of Biomedical Engineering, Science and Health Systems, Philadelphia, Pennsylvania, 19104 USA. shihwy@drexel.edu

Abstract

We have examined *in situ* detection of single-nucleotide *KRAS* mutation in urine using a $(Pb(Mg_{1/3}Nb_{2/3})O_3)_{0.65}(PbTiO_3)_{0.35}$ (PMN-PT) piezoelectric plate sensor (PEPS) coated with a 17-nucleotide (nt) locked nucleic acid (LNA) probe DNA complementary to the *KRAS* mutation. To enhance *in situ* mutant (MT) DNA detection specificity against the wild type (WT), the detection was carried out in a flow with a flow rate of 4 mL/min and at 63°C with the PEPS vertically situated at the center of the flow in which both the temperature and the flow impingement force discriminated the wild type. Under such conditions, PEPS was shown to specifically detect *KRAS* MT *in situ* with 60 copies/mL analytical sensitivity in a background of clinically-relevant 1000-fold more WT in 30 min without DNA isolation, amplification, or labeling. For validation, the detection was followed with detection in a mixture of blue MT fluorescent reporter microspheres (FRMs) (MT FRMs) that bound to only the captured MT and orange WT FRMs that bound to only the captured WT. Microscopic examinations showed that the captured blue MT FRMs still outnumbered the orange WT FRMs by a factor of 4 to 1 even though WT was 1000-fold of MT in urine. Finally, multiplexed specific mutation detection was demonstrated using a 6-PEPS array each with a probe DNA targeting one of the 6 codon-12 *KRAS* mutations.

Introduction

Cancer is a genetic disease and gene mutation is an important form of genetic defects that play a central role in cancer pathways. Detecting gene mutation is essential for cancer diagnosis, therapy decision, and therapy efficacy monitoring. The challenge for gene sequencing from solid tumor samples is that therapeutic decision making based on a single biopsy can be very difficult due to tumoural heterogeneity[1]. Furthermore, the biopsy

† Footnotes relating to the title and/or authors should appear here.

Electronic Supplementary Information (ESI) available: [details of any supplementary information available should be included here]. See DOI: 10.1039/x0xx00000x

procedures used for removing tissues from cancers of the internal organs are highly intrusive and expensive and not performed in some cases due to the increased risk of tumour seeding to other sites[2]. These shortcomings make it highly desirable if body fluids such as blood or urine can be used for cancer genetic marker detection.

Polymerase chain reaction (PCR) has been the method of detecting circulating deoxyribonucleic acid (DNA) markers in serum or urine. To detect gene mutation, PCR is typically followed with melting temperature analysis to differentiate mutant (MT) from the wild type (WT), the normal form of the gene. So far, detecting mutations in sera or urine has been challenging because (1) the melting-temperature difference between a single-nucleotide MT and the WT can be only a few degrees[3], (2) the concentrations of circulating MT markers are exceedingly low (much lower than 10^{-18} M or 600 copies/mL)[4], (3) circulating MT markers are typically outnumbered by the WT by a factor of 240 or larger[5], (4) trans-renal DNA exist in urine in the form of short fragments often less than 200 base pairs (bp)[6], and PCR suffers from amplicon size, where only a small amount of the naturally occurring fragments in urine can be amplified.[5, 7] These combinations make it difficult to detect circulating mutations sensitively and specifically. Therefore, if there is a genetic detection method that can detect genetic mutations in short DNA fragments of less than 200 bp at concentrations lower than aM (10^{-18} M) and in a background of more than 240-fold wild type (WT) without the need of DNA isolation or amplification it would be ideal for reliably detecting circulating genetic mutations in urine that can greatly help cancer diagnostics and treatment decision and monitoring.

Genetic detection technologies currently under development rely fluorescence[8], quartz crystal microbalance (QCM)[9, 10], electrochemical[11], binding to nano-metal particles[12], surface plasmon resonance (SPR)[13], silicon-based microcantilever sensor as well as piezoelectric microcantilever sensor. For DNA detection, nanoparticle-amplified QCM exhibited a concentration sensitivity of 1 pM[14]. Nanoparticle enhanced SPR exhibited concentration sensitivity of 10-100 aM[15]. The electrochemical methods involving nanofibers and nanotubes also exhibited concentration sensitivity on the order of 30 fM[16]. Nanowires[17-21], and nanotubes[22, 23] exhibited concentration sensitivity ranging from 100 fM to 1 fM. Microcantilevers coupled with nano-metal particles exhibited 0.01 nM concentration sensitivity[24]. Although many of these methods such as QCM, SPR, silicon-based microcantilever sensor as well as lead zirconate titanate (PZT) piezoelectric microcantilever sensor (PEMS)[25, 26] are label-free, the sensitivity was still many orders of magnitude away from the attomolar (aM, or 10^{-18}M) requirement. Similarly, the 10^{-16} M sensitivity achieved by magnetic beads isolation coupled with electrochemical enhancement was still not sufficient[27]. Nano-scale mechanical imaging by atomic force microscopy (AFM) could differentiate unhybridized single-stranded DNAs (ssDNAs) from hybridized double-stranded DNAs (dsDNAs) at aM sensitivity but it required sophisticated instrument such as AFM[28]. Carbon nanotube impedance biosensors exhibited 100 aM sensitivity in DNA detection, which was insufficient for clinical applications[29]. GaN nanowire extended-gate field-effect-transistors[30] and streptavidin horseradish peroxidase functionalized carbon nanotubes[31] have aM sensitivity in DNA detection. However, these detections are not in situ they typically require washing steps before the measurements can be made. Peptide nucleic acid (PNA) probe-enhanced electrochemical biosensors that were based on an integrated

chip also exhibited aM sensitivity. However, they also required washing [32]. Recently a disposable electrochemical biosensor based on magnetic bead amplification and target DNA biotinylation exhibited aM sensitivity[33]. However, it required multiple steps of amplification and the need to biotinylate the target DNA render it impractical[33]. In comparison with these technologies, the limit of detection (LOD) of a piezoelectric plate sensor PEPS in urine exceeds the attomolar level requirement while also label-free. Moreover detection with PEPS proved enough specificity for Mutant target DNA on a background of 250 times more Wild Type target DNA.[34]

A lead magnesium niobate–lead titanate $(Pb(Mg_{1/3}Nb_{2/3})O_3)_{0.65}(PbTiO_3)_{0.35}$ (PMN-PT) piezoelectric plate sensor (PEPS) consists of a PMN-PT freestanding film 8 μm in thickness[35] thinly coated with gold electrodes on the two major surfaces and encapsulated with a thin electrical insulation. By covalently immobilizing a probe DNA (probe) complementary to a target DNA and immersing the probe-coated PEPS in a biological fluid sample, binding of the target DNA from the biological fluid sample to the probe on PEPS surface shifts the PEPS length extension mode (LEM) and width extension mode (WEM) resonance frequency, f. *In situ* detection of the target DNA from the biological fluid sample has been achieved by monitoring the PEPS LEM [36] or WEM[37] resonance frequency shift, Δf in real time. The detection signal of PEPS is mainly from the response to surface stress which is larger than the response to mass change by more than 1000 times. The reason for the large response to surface stress is that PEPS can switch its crystalline orientation under the influence of surface stress, which no other materials can. Because the elastic moduli of crystalline materials are orientation-dependent, the resultant elastic modulus change causes a resonance frequency shift more than 1000 times higher than could be obtained by the mass change alone [36, 38-42]. Using 200-neocleotide (nt) Hepatitis B virus 1762T/1764A double mutation (HBVDM) as a model single-stranded MT, PEPS has exhibited unprecedented PCR-like 100 zM (10^{-19}M) analytical sensitivity in detecting HBVDM in urine in situ and in real time without DNA isolation or amplification.[37].

In view of the high sensitivity and specificity demonstrated by a PEPS in detecting HBVDM which contains two point mutations separated by one nucleotide, the goal of this study is to further investigate the specificity of in situ single-nucleotide mutation in urine against the WT in real time using a PEPS with locked nucleic acid (LNA) probe in a flow and with temperature control but without DNA isolation or amplification. *KRAS* mutations are point mutations at codons 12 and 13 and less frequently at codon 61 that occur in about 50% of colorectal cancers[43] and more than 80% of pancreatic cancers [44]. Among the seven most common *KRAS* mutations, codon-12 GGT to GTT point mutation (Glycine to Valine) (G12V) is associated with a higher mortality rate[45]. Frequency of this mutation among *KRAS* mutated colorectal cancers is 21.9-24.4% [46]. In this study we will use the *KRAS* G12V PM as the model PM. Specifically, we will use a 50-nt *KRAS* PM as the model MT. Hybrid probes containing both DNA and locked nucleic acid (LNA) nucleotides have been shown to increase the melting-temperature difference between the MT and WT and enhance the specificity of mutation detection [47-54].

For the GGT-to-GTT *KRAS* mutation, we designed and immobilized an LNA-containing probe on the PEPS surface to carry out in situ *KRAS* PM MT detection against the WT at a

temperature below the melting temperature of the MT but above that of the WT and with a flow rate of 4 mL/min. We showed that the PEPS positively and specifically detected the *KRAS* G12V PM MT at a concentration of 60 copies/mL (100zM, or 10^{-19}M) in a background of 1000-fold WT and further validated the MT detection by following with in situ fluorescent reporter microspheres (FRMs) detection and by visualizing the fluorescent colors of FRMs. The numbers of captured MT FRMs outnumbered the captured WT FRMs by a factor of 4 to 1, indicating the specificity of PEPS single-nucleotide PM detection even when the samples contains 1000-fold WT.

Experimental

Probe, MT, WT, rDNAs and FRMs

The 17-nt LNA probe used to detect the *KRAS* G12V PM MT was a synthetic single-stranded DNA (Exiqon) complementary to the sequence of the *KRAS* gene (Gene ID: 3845) centered around the *KRAS* G12V PM with the 3 LNA bases also centered around the PM as shown in Table I. Such a design has been shown to increase the melting-temperature difference between the binding of the MT to the probe and that of the WT to the probe[55]. Without using the 3 LNA bases, the melting temperatures for the MT and the WT would be 62°C and 52°C, respectively with a melting temperature difference of 10°C. With the 3 LNA bases, the melting temperature for the MT was 70°C and that for the WT 55°C. The melting-temperature difference between the MT and the WT was thus increased from 10°C to 15°C. The probe was amine- activated with a 12-polyethyleneglycol (PEG) spacer at the 5′ end. The sequence of the probe is shown in Table I. The MT and WT were 50-nt long synthetic single-stranded DNA (Sigma). The MT contained the sequence complementary to the probe (in black in Table I) plus 33 nt of the immediately upstream sequence (in blue in Table I) while the WT contained the sequence complementary to the probe (in black in Table I) except for the point mismatch plus 33 nt of the immediately downstream sequence (in green in Table I). Also shown in Table I is the sequence of the rDNA for MT (MTrDNA) which was complementary to the upstream sequence of the MT shown in blue in Table I and sequence of the rDNA for WT (WTrDNA) complementary to the downstream sequence of the WT shown in green in Table I. Both MTrDNA and WTrDNA were 33-nt long (Sigma). The WTrDNA was amine activated with a 12-PEG spacer at the 5′ end and the MTrDNA was also amine activated but with a 7-PEG spacer at the 3′ end. Also shown in Table I are the melting temperature (T_m) for the binding of the MT with the probe, that for the binding of the WT with the probe, that for the MTrDNA to MT, and that for the WTrDNA to WT. MTrDNA and WTrDNA were covalently conjugated to the MT FRMs and WT FRMs, respectively. Both MT and WT FRMs were 6 μm in size but differed in the fluorescent color. MT FRMs emitted blue light (Bright Blue (BB) (≈ Coumarin), Polysciences) with excitation maximum at 360 nm and emission maximum at 407 nm whereas the WT FRMS emitted yellow-green light (Yellow Green (YG) (≈ Fluorescein), Polysciences) with excitation maximum at 441 nm and emission maximum at 486 nm. Fig. 1 shows a schematic illustrating the relationship between probe, MT, WT, MTrDNA, WTrDNA, MT FRMs, and WT FRMs. As can be seen, the sequences of MT, WT, MTrDNA, and WTrDNA were chosen such that the MT FRMs would report only the presence of MT and the WT FRMs would report only the presence of WT. For this purpose, after FRMs detection, two

fluorescent images of the PEPS surface were taken using an Olympus BX51 fluorescent microscope using the imaging procedure described earlier [58]. One image contained only the MT FRMs by using a D350/50 filter (Chroma) for excitation and a 400 nm long-pass filter (Chroma) for emission while the other image contained only the WT FRMs by using a D460/50 filter (Chroma) for excitation and a HQ545/30 filter (Chroma) for emission. Even though the MT FRMs images were taken with a 400 long pass emission filter, they did not contain the images of WT FRMs because the WT FRMs could not be excited with the D350/50 excitation filter. For the latter image, a longer exposure time was used to make up for the fact that the emission filter did not completely overlap with the emission spectrum of the WT FRMs. The fluorescent spots in the MT FRMs image were then colored blue to denote that they are MT FRMs and those in the WT FRMs image were then colored orange to denote that they are WT FRMs using MatLab. After coloring, the blue and orange images were merged using MatLab. Because MT FRMS and WT FRMS exhibited different fluorescent colors, by examining the colors of the FRMs captured on the PEPS surface following MT detection in a mixture of MT and WT, one could determine how specific the MT detection was in a background of WT.

PEPS fabrication and electrical insulation

The PEPS used in this study was 1.2 mm long and 0.45 mm wide fabricated from $(PbMg_{1/3}Nb_{2/3}O_3)_{0.65}$-$(PbTiO_3)_{0.35}$ (PMN-PT) freestanding films 8 μm thickness that was coated with 110 nm thick Cr/Au electrode by thermal deposition (Thermionics VE 90) cut into 2.5 mm by 0.45 mm strips by a wire saw (Princeton Scientific Precision, Princeton, NJ) as shown in Fig. 2a. Gold wires, 10 μm in diameter, were glued to the top and bottom electrodes of each strip using conductive glue (XCE 3104XL, Emerson and Cuming Company, Billerica, MA). The rear end of the strip was fixed on a glass substrate by a nonconductive glue (Loctite 1C Hysol Epoxy Adhesive) to form the PEPS geometry and poled at 15KV/cm at 90°C for 60 min in an incubator (Digital Control Steel Door Incubator 10-180E, Quincy Lab). The dielectric constant of the PEPS was measured using an electrical impedance analyzer (Agilent 4294A) to be about 1800 with a loss factor of 2.8% at 1 kHz. The PEPS was electrically insulated to stabilize the resonance peaks for in-liquid detection by using a new 3-mercaptopropyltrimethoxysilane (MPS) (Sigma-Aldrich Co. LLC.) solutions coating scheme involving enhanced MPS cross-linking at pH=9.0 and with the addition of water as described before[59]. The MPS insulation also served as the anchor to immobilize the probe via the bi-functional linker SMCC. The pKa of thiols is about 10.5. Under the coating conditions at pH=9.0 or the immobilization conditions at pH=7, most of the thiols were un-oxidized and good for the immobilization. Indeed, the probe immobilized on the MPS surface was quantified using quartz crystal microbalance (QCM) to be about 3-4 probes per 100 nm^2.[60] Thus, the SH of the MPS was proven to be effective to facilitate the immobilization of the probe DNA. A schematic of LEM vibrations and that of WEM vibrations of a PEPS are shown in the insert (I) and (II) of Figs. 2b, respectively. The impedance (blue) and phase angle (red) versus frequency resonance spectra around the first WEM peak frequency--which was taken as the peak frequency of the phase angle versus frequency spectrum--are shown in Fig. 2b. Because the phase-angle resonance spectrum was much more symmetric than that of the impedance, in the following, all detections were carried out using the phase-angle spectrum to track the WEM peak.

Probe immobilization, nonspecific binding blocking, and FRMs conjugation

Sulfosuccinimidyl-4-(N-maleimidomethyl)cyclohexane-1-carboxylate (sulfo-SMCC) (Pierce) was first dissolved in water followed by dilution in a phosphate buffer saline (PBS) solution. To immobilize the amine-activated probe on the PEPS surface, the MPS-coated PEPS was first immersed in 200μL of a 5 mM sulfo-SMCC solution in PBS with the pH adjusted to 6.5 for 1 hour. The sensor was then washed three times with deionized water and then it was immersed in a solution of 10 μM of amine activated probe dissolved in 200 μL of PBS (pH 8.0). A schematic illustrating the immobilization of the amine-activated probe on the PEPS surface via the thiol functionality of the MPS insulation layer is shown in Fig. S1 of the supplemental information. After probe immobilization, the PEPS was treated with 3% bovine serum albumin (Sigma) in PBS for 1 hr followed by washing 5 times with PBS. As demonstrated by the previous study, 3% BSA was sufficient to completely block the nonspecific bindings for DNA detection in urine.[37] The MT FRMs were covalently conjugated to MTrDNA and the WT FRMS to the WTrDNA using procedures described previously.[36, 58] The total volume of MT FRMs solution was 8 mL and the concentration was 1×10^5 FRMs/mL. At 2 mL/min, this solution was recycled approximately 7 times in the 30 minutes of the MT FRMs detection step. The likely reason for the fact that the detection of the 50 nt MT/WT produced quite similar Δf/f to that of the detection of the larger MT FRMs/WT FRMs is the following. DNA was highly negatively charged--including the probe DNA on the PEPS surface, MT, WT and the reporter DNA on the FRMs surface. Therefore, much of the surface stress generated by MT, WT or FRMs binding was due to the electrostatic repulsive forces between the negatively charged surface due to the immobilized probe DNA layer and the negatively charged target (MT, WT or FRMs). Under physiological electrolyte concentrations, the electrical screening length (or electrical double layer thickness) is less than 1 nm. This means that charges at a distance more than 1 nm away from the probe DNA layer would generate negligible repulsive forces on the probe DNA layer, hence the PEPS surface. As a result, most of a bound FRM did not contribute to the surface stress except the vicinity at and around the binding site that was right on the probe DNA layer. Note that a 6-μm FRM generated comparable resonance frequency shift to that of a 50 nt MT or WT is another indication that PEPS sensing mechanism is not by mass change.

Spiked urine samples and flow setup

The flow system for carrying out the detection contained a peristaltic pump (Cole-Parmer 77120 – 62), a flow cell where detection took place, reservoirs containing DNA-spiked urine samples, FRMs, and PBS interconnected with tubing of a 0.8-mm inner diameter as schematically shown in Fig. 1c. The flow cell was 18.5 mm long, 3.5 mm wide and 5.5 mm deep (volume = 356 μL) connected to the sample reservoir. A schematic of the flow cell is shown in Fig. 1d. The total internal volume of the flow cell plus tubing was approximately 750 μL. The urine came from one individual. The subject was free of HBV infection. The urine samples were collected in a “First Morning Specimen” manner, i.e., the bladder was emptied before bed and the sample was collected first thing in the morning. A total of 11 such urine samples were collected for the study and visually there was no significant difference among these 11 urine samples and 21 more that were used for previous studies [34, 37]. The flow was driven by the peristaltic pump and what flowed through the flow

cell was controlled by the valves. In each detection experiment, the volume of the DNA-spiked urine sample was fixed at 50 mL and the probe-coated PEPS was placed in the center of the flow cell. The flow setup was placed inside an incubator (Digital Control Steel Door Incubator 10-180E, Quincy Lab) for temperature control. Because the flow cell was open a 2-litre water bath was included in the incubator to eliminate potential resonance frequency shift due to the changes in the flow-cell liquid level by evaporation. The resonance spectra were measured using a portable AIM 4170 C impedance analyzer (Array Solutions).

Results and Discussion

Single-PEPS Mutation Detection

An optical micrograph of the PEPS used for this study is shown as an insert in Fig. 2c. The in-air and in-PBS phase angle versus frequency resonance spectra of the PEPS are shown in Fig. 2c. As can be seen, the base-line, the length-extension-mode (LEM) resonance peak, and the width-extension-mode resonance (WEM) peak of the in-liquid spectrum were close to those of the in-air spectrum, indicating the effectiveness of the MPS insulation coating. In all of the following experiments, the WEM peak of the phase-angle spectrum was monitored for detection. The relative resonance frequency shift, Δf/f, of the first WEM peak during the SMCC bonding (30-60 min), the probe immobilization (60-90 min), the subsequent MT detection at 100 pM in PBS (90-120 min) and the following MT FRMs detection at 1×10^5 FRMs/mL concentration in PBS (120-150 min), both a 2 mL/min is shown in Fig. 2d. Also shown in the insert in Figure 2d is a schematic of the various steps involved in the immobilization process. Fig. 2d was done in PBS at room temperature mainly to illustrate the various binding steps during surface functionalization, MT detection or FRM validation could be detected by the resonance frequency shift of the PEPS. For actual MT or WT detection in urine, there was a bovine serum albumin (BSA) blocking step right after probe immobilization in which the probe-coated PEPS was treated with a 3% BSA solution for 30 min to saturate any possible nonspecific binding sites such that no nonspecific binding could occur during detection in urine as described earlier [37].

With the melting temperature for the binding of the MT to the probe being 70°C and that for the WT to the probe being 55°C, we carried out the detection of 1×10^{-15} M of MT and WT in PBS at 55°C, 60°C, 63°C and 68°C for 30 min to find the optimal temperature for specific MT detection against the WT. Three experiments were carried for each condition. The resultant relative detection resonance frequency shift, Δf/f is plotted with standard deviations in Fig. 2e. We then averaged out the Δf/f of each detection over 25-30 min. The resultant -Δf/f at 25-30 min is plotted in Fig. 2f with squares representing MT and circles representing WT (the left side of the double-y plot). The ratio of the −Δf/f at 25-30 min of the MT to that of the WT is also plotted in Fig. 2f as the triangles (the right side of the double-y plot). As can be seen the ratio of the −Δf/f at 25-30 min of the MT to that of the WT was maximal at 63°C. Figs. 3a and 3b show the schematic of the MT detection in urine and that of the following MT FRMs detection, respectively. Fig. 3c shows the detection Δf/f versus time of the MT detection in urine at various MT concentrations followed by the MT FRMs detection in PBS at 1×10^5 FRMs/mL. Note the background signal in blank urine (control) before and after the MT and FRM detection steps were stable as shown in Fig. 3c in all the detection

experiments. For simplicity, in all the following figures we will omit the background signal sections to better highlight the detection results. Figs. 3d and 3e show the schematic of the WT detection in urine and that of the following detection of the WT FRMs in PBS, respectively. Fig. 3f shows the detection $-\Delta f/f$ versus time in urine at various MT concentrations followed by the detection of the WT FRMs in PBS at 1×10^5 FRMs/mL. Clearly, the detection $-\Delta f/f$ for MT at 1 aM (1×10^{-18} M) at t = 30 min was about 0.2×10^{-3}, which was still larger than the detection $-\Delta f/f$ of $<0.1\times10^{-3}$ for WT at 100 fM (1×10^{-14} M) at t = 30 min, indicating the specificity of the MT detection by PEPS at the chosen detection conditions of 63°C and 4 mL/min flow rate.

To see if PEPS detection of *KRAS* MT under the current detection conditions, i.e., 63°C and a flow rate of 4 mL/min was indeed sensitive and specific, we carried out MT detection in a background of 1000-fold higher WT at various MT concentrations. In Fig. 4a, we show the $\Delta f/f$ versus time of PEPS detection in urine containing a mixture of MT in a background of 1000-fold more WT at various MT concentrations followed by detection in an equal mixture of 10^5 FRMs/mL of MT FRMs and 10^5 FRMs/mL of WT FRMs in PBS.

After the detection in the mixture of MT FRMs and WT FRMs and washing, the PEPS was examined using a fluorescent microscope and the obtained fluorescent images from detection at various MT concentrations are shown in Figs. 4b-4e where the blue spots represent the MT FRMs and the orange ones WT FRMs. As can be seen, in all four MT concentrations (i.e., 100 zM, 1 aM, 10 aM and 100 aM) the blue MT FRMs outnumbered the orange WT FRMs. In addition, both the number of MT FRMs and that of the WT FRMs increased with an increasing MT concentration since the WT concentration was increased in proportion as well. In Fig. 5a, we plot the number of MT FRMs and that of WT FRMs versus the average $-\Delta f/f$ of MT detection in a MT/WT mixture as obtained from the $-\Delta f/f$ at t = 25-30 min in Fig. 4a. Clearly, both the number of the MT FRMs and that of the WT FRMs increased roughly linearly with an increasing average $-\Delta f/f$ of MT detection with a MT FRMs/WT FRMs number ratio of about 4, validating that the $\Delta f/f$ obtained in a MT/WT mixture with a WT/MT ratio of 1000 was mostly due to the binding of MT on the PEPS surface such that the bound FRMs were mostly MT FRMs. These results are schematically illustrated in Figs. 4f-4h. Fig. 4f illustrates that even in a mixture of MT with 1000-fold more WT, still more MT than WT were captured on the PEPS surface because the temperature and flow condition favored MT to bind to the probe on the PEPS surface. Fig. 4g illustrates that in detection in an equal mixture of MT FRMs and WT FRMs following the detection in the mixture of MT with 1000-fold more WT, more MT FRMS would bond on the PEPS surface due to more MT captured on the PEPS surface. Fig. 4h illustrates that the final PEPS surface had more bound MT FRMs with a MT FRMs/ WT FRMs number ratio of about 4 after detection in the equal mixture of MT FRMs and WT FRMs and washing.

To see how the detection of MT in a background of 1000-fold WT shown in Figs. 4a compared with detection in pure MT and that in pure WT in Figs. 3c and 3f, we plot in Fig. 5b the average $-\Delta f/f$ over t = 25-30 min at 10^{-19} M, 10^{-18} M, and 10^{-17} M in pure MT (black) as obtained from Fig. 3c, that at 1000-fold WT (red) as obtained from Fig. 3f, and that in a mixture of MT with 1000-fold WT (blue) as obtained from Fig. 4a (blue). As can be

seen from Fig. 5b, the overall detection −Δf/f in a mixture (blue) was somewhat smaller than that of pure MT detection at the same concentration (black), understandably due to the interference by the presence of the 1000-fold WT except at low concentrations where WT had a negligible effect due to the low concentrations.

Note in Fig. 5b, the −Δf/f of the pure MT detection (black) of all three concentrations were also roughly 4 times that of the pure WT detection at a 1000-fold higher concentration, consistent with the results from the detection in MT/WT mixture shown in Fig. 5a and further supporting that under the detection conditions of 63°C and 4 mL/min, roughly 80% (4 out of 5) of the detection signals were due to MT even in a background of 1000-fold WT.

Example of 6-PEPS Array Mutation Detection

Codon 12 and codon 13 are hot spots of *KRAS* mutations. Six codon-12 mutations and one condon-12 (G13D) account for more than 98% of all *KRAS* mutations. For the initial demonstration of the PEPS capability of multiplexed mutation detection, we constructed an array of six PEPSs to target the 6 codon-12 hot-spot *KRAS* mutations. The resonance spectra of the 6 PEPSs are shown in Fig. S2 in the supplemental information. In Table II, we list the six condon-12 *KRAS* mutations, the corresponding LNA probe sequences (Exiqon), the melting temperature between the probe and its target MT and that between the probe and the WT. The 6 synthetic codon-12 MTs were single-stranded and 90-nt long (Integrated DNA Technologies). The melting temperatures for the MTs ranged from 68°C to 72°C and those of the WTs ranged 50.1°C to 54.3°C with melting temperature differences ranging 15.3°C to 20.9°C. Each PEPS was coated with a different LNA probe as specified in Table II. The immobilization of each biotin-activated probe to each corresponding PEPS was carried out using the procedures described previously.[37] The detection of each MT using the 6-PEPS was carried out at 63°C, a temperature midway between the melting temperatures of all the MT and those of the WT and with a flow rate of 4 mL/min. Multichannel measurement was accomplished by multiplexing 6 sensors using 1 impedance analyzer and two relay modules (Super4 USB Relay Module, TCTEC Pty Ltd, Australia). The 6 PEPS are cycled through the impedance analyzer via the 2 relay modules. The setup was calibrated to exclude the contribution from the relay modules to the complex impedance of the sensor. A Matlab routine was written to control the relay modules to switch between different PEPSs automatically. Solutions for 6 different target DNAs were prepared separately and flown through the two flow cells in series each containing 3 PEPSs where each PEPS had a different probe immobilized on its surface as illustrated by the different colors on the PEPS surface as shown in Fig. 6a. Although the multiplexed detection was carried out in urine samples spiked with only one type of MT, it is carried out with the ability to read out all six probes at the same time. In each detection event, only one probe has positive response while all five other probes have negative responses, indicative of the accuracy and specificity of the probes. The detection data of each PEPS were collected, analyzed and displayed in real time using the MatLab program in the same way as with a single PEPS. In each detection event, the urine was spiked with only one MT at 100 aM (10^{-16} M). Thus, only the PEPS coated with the complementary probe could detect the MT. Indeed, in Fig. 6b, we show the Δf/f versus time of the multiplexed detection where there were six Δf/f versus time plots stacked vertically from (i) to (vi), each plot representing the Δf/f versus time of one PEPS

(PEPS1 to PEPS6). The six detection events were run successively with each event lasting for 30 min. The 6 detection events were denoted by 6 different colors in the plots. As can be seen, each PEPS detected only one mutation but not the others. This example clearly illustrates that array PEPS could perform multiplexed test to allow all possible forms of the codon-12 mutations to be detected in one single test.

Discussions

There are two types of point mutations, transitions that have no pyrimidine/purine substitutions and transversions with pyrimidine/purine substitutions. Four of the six codon-12 KRAS mutations (G12S, G12D, G12V, and G12C) were transitions and the other two were transversions (G12R and G12A) with a purine substitution of pyrimidine. Using similar probe design considerations such as the number of LNAs, the two transversions had a wider melting temperature spread between MT and WT than the four transitions (see Table II). In this case, using one of the four transitions, G12V as the model was sufficient to ensure that the same mutation detection methodology could be applied to the two transversions with similar mutation detection specificity as illustrated in the multiplexed detection of all 6 codon-12 KRAS mutations in Fig. 6. For transversions with a pyrimidine substitution of purine which the current study did not consider, using a LNA probe design similar to what was used in the current study could result in a smaller Tm spread between MT and WT. In that case, to widen the Tm spread of such transversions, the LNA probe could be redesigned with a different number of LNAs as well as different locations of the LNAs to allow a Tm spread of 15°C. With that, the same mutation detection methodology could be applied to such transversions with similar mutation detection specificity illustrated in this study.

The current probe was only 17-nt long with the mutated site in the middle (9^{th}-nt), as long as the mutation site of a target MT is 8-nt or more from the edge of the target DNA, the binding of the probe to the target MT will have the expected melting temperature of 70°C. In urine most of the tumor derived cell free DNA fragments are low molecular weight (200 bp)[6]. The probability for the mutated site to be within 8 nt of either end would therefore be less than 8% on average. Thus, the current 17-nt probe would bind to the DNA fragments in urine with a probability of better than 92%. In comparison, PCR needs two primers and one probe, thus would not be able to detect a MT with a mutation site as far off the center as 8 nt away from the edge. Conservatively assuming the two primers and the probe to be all 17-nt long, for the MT to be detectable, the mutation site must be 25-nt or more away from the edge, reducing the chances of detecting the MT to 75%. Most of the primer and probe sequences in PCR are much longer than 17-nt long, which will further reduce the chance of detecting the mutation from the fragments. Clearly, the current method needs only a short probe is an advantage over PCR in detecting mutations from circulating DNA fragments.

The same methodology should also be able to detect mutations in circulating DNA from plasma or serum. The only difference is that the sensor must be blocked with a higher concentration of bovine serum albumin (BSA) after probe immobilization and prior to detection to prevent non-specific binding as plasma and sera contain higher concentrations of serum albumin.[60]

The current hybridization temperature is not high enough to denature dsDNA. Detection of dsDNA will require denaturing the dsDNA prior to hybridization, which can be incorporated in the flow system in a continuous fashion and will be published in future publication. Finally, the current hybridization temperature is not high enough to denature dsDNA. Detection of dsDNA will require denaturing the dsDNA first prior to hybridization. Both the denature step and the hybridization step could be incorporated in the flow system in a continuous fashion and will be published in future publication.

Conclusion

We have examined the analytical sensitivity and selectivity of *in situ* detection of gene mutation in urine using a PMN-PT PEPS using *KRAS* G12V point mutation (PM) as the model PM. The PEPS was coated with a 17-nt probe with three LNA bases around the mutated site that was complementary to the *KRAS* PM and the detection was carried out in a flow with the PEPS located at the center of the flow with a flow rate of 4 mL/min and at 63°C which was below the melting temperature of the MT with the probe but above that of the WT with the probe. To examine the specificity of the mutation detection in a background of wild type, we follow the detection in the mixture of MT and WT with detection in a mixture of MT FRMs and WT FRMs in which MT FRMS and WT FRMS were designed to bind only to MT and WT, respectively. The specificity can be further confirmed by visual inspection of the colors of the bound FRMs as the MT and WT FRMs emitted different fluorescent colors. The results indicated that under the optimal detection conditions of 63°C and 4 mL/min, PEPS detected the *KRAS* PM with an analytical sensitivity of 60 copies/mL in urine in a background of 1000-fold more WT without DNA isolation or amplification. Counting the captured MT FRMs and WT FRMs after the following FRMs detection indicated that roughly 80% (4/5) of the detection signals were due to the MT even in the presence of 1000-fold more WT. Multiplexed mutation detection was demonstrated using a 6-PEPS array each with a probe complementary of one of the 6 codon-12 *KRAS* mutations.

Supplementary Material

Refer to Web version on PubMed Central for supplementary material.

Acknowledgment

This work was supported in part by the Coulter-Drexel Translational Research Partnership grant, the Nanotechnology Institute of Benjamin Franklin Partnership of Southeastern Pennsylvania, and National Institute of Health Grants No. 1R41AI1122224 and 1R41AI120445.

Notes and references

1. Crowley E, Di Nicolantonio F, Loupakis F, Bardelli A. Nat Rev Clin Oncol. 2013; 10:472–484. [PubMed: 23836314]
2. Robertson EG, Baxter G. Clinical radiology. 2011; 66:1007–1014. [PubMed: 21784421]
3. Lipsky RH, Mazzanti CM, Rudolph JG, Xu K, Vyas G, Bozak D, Radel MQ, Goldman D. Clin Chem. 2001; 47:635–644. [PubMed: 11274012]
4. Caruso F, Rodda E, Furlong DN, Niikura K, Okahata Y. Analytical Chemistry. 1997; 69:2043–2049. [PubMed: 21639244]

5. Su YH, Wang M, Block TM, Landt O, Botezatu I, Serdyuk O, Lichtenstein A, Melkonyan H, Tomei LD, Umansky S. Ann N Y Acad Sci. 2004; 1022:81–89. [PubMed: 15251944]
6. Su YH, Wang MJ, Brenner DE, Ng A, Melkonyan H, Umansky S, Syngal S, Block TM. Journal of Molecular Diagnostics. 2004; 6:101–107. [PubMed: 15096565]
7. Umansky SR, Tomei LD. Expert Rev Mol Diagn. 2006; 6:153–163. [PubMed: 16512776]
8. Hammond DM, Manetto A, Gierlich J, Azov VA, Gramlich PM, Burley GA, Maul M, Carell T. Angew Chem Int Ed Engl. 2007; 46:4184–4187. [PubMed: 17458844]
9. Passamano M, Pighini M. Sensors and Actuators B: Chemical. 2006; 118:177–181.
10. Feng K, Li J, Jiang JH, Shen GL, Yu RQ. Biosens Bioelectron. 2007; 22:1651–1657. [PubMed: 16963256]
11. Gasparac R, Taft BJ, Lapierre-Devlin MA, Lazareck AD, Xu JM, Kelley SO. Journal of the American Chemical Society. 2004; 126:12270–12271. [PubMed: 15453752]
12. Park SJ, Taton TA, Mirkin CA. Science. 2002; 295:1503–1506. [PubMed: 11859188]
13. He L, Musick MD, Nicewarner SR, Salinas FG, Benkovic SJ, Natan MJ, Keating CD. Journal of the American Chemical Society. 2000; 122:9071–9077.
14. Mao X, Yang L, Su XL, Li Y. Biosens Bioelectron. 2006; 21:1178–1185. [PubMed: 15951163]
15. Gifford LK, Sendroiu IE, Corn RM, Luptak A. J Am Chem Soc. 2010; 132:9265–9267. [PubMed: 20565098]
16. Yang T, Zhou N, Zhang Y, Zhang W, Jiao K, Li G. Biosens Bioelectron. 2009; 24:2165–2170. [PubMed: 19131238]
17. Zheng G, Patolsky F, Cui Y, Wang WU, Lieber CM. Nat Biotechnol. 2005; 23:1294–1301. [PubMed: 16170313]
18. Zhang GJ, Luo ZH, Huang MJ, Tay GK, Lim EJ. Biosens Bioelectron. 2010; 25:2447–2453. [PubMed: 20435462]
19. Andreu A, Merkert JW, Lecaros LA, Broglin BL, Brazell JT, El-Kouedi M. Sensors and Actuators B: Chemical. 2006; 114:1116–1120.
20. Gao Z, Agarwal A, Trigg AD, Singh N, Fang C, Tung CH, Fan Y, Buddharaju KD, Kong J. Anal Chem. 2007; 79:3291–3297. [PubMed: 17407259]
21. Hahm, J.-i.; Lieber, CM. Nano Letters. 2003; 4:51–54.
22. Wang J, Polsky R, Merkoci A, Turner KL. Langmuir. 2003; 19:989–991.
23. Chang H, Yuan Y, Shi N, Guan Y. Anal Chem. 2007; 79:5111–5115. [PubMed: 17530821]
24. Su M, Li S, Dravid VP. Applied Physics Letters. 2003; 82:3562–3564.
25. Rijal K, Mutharasan R. Anal Chem. 2007; 79:7392–7400. [PubMed: 17764156]
26. Zheng S, Choi JH, Lee SM, Hwang KS, Kim SK, Kim TS. Lab on a Chip. 2011; 11:63–69. [PubMed: 21060947]
27. Wang J, Kawde AN, Musameh M. Analyst. 2003; 128:912–916. [PubMed: 12894830]
28. Husale S, Persson HH, Sahin O. Nature. 2009; 462:1075–1078. [PubMed: 20010806]
29. Kurkina T, Vlandas A, Ahmad A, Kern K, Balasubramanian K. Angew Chem Int Ed Engl. 2011; 50:3710–3714. [PubMed: 21425218]
30. Chen C-P, Ganguly A, Lu C-Y, Chen T-Y, Kuo C-C, Chen R-S, Tu W-H, Fischer WB, Chen K-H, Chen L-C. Anal Chem. 2011; 83:1938–1943. [PubMed: 21351780]
31. Gao W, Dong H, Lei J, Ji H, Ju H. Chem Commun (Camb). 2011; 47:5220–5222. [PubMed: 21461429]
32. Soleymani L, Fang Z, Kelley SO, Sargent EH. Applied Physics Letters. 2009; 95:143701–143703.
33. Loaiza OA, Campuzano S, Pedrero M, Pividori MI, Garcia P, Pingarron JM. Anal Chem. 2008; 80:8239–8245. [PubMed: 18837513]
34. Kirimli CE, Shih W-H, Shih WY. Analyst. 2015
35. Shih WY, Luo H, Li H, Martorano C, Shih W-H. Applied Physics Letters. 2006; 89:242913–242913.
36. Wu W, Kirimli CE, Shih WH, Shih WY. Biosens Bioelectron. 2013; 43:391–399. [PubMed: 23356996]
37. Kirimli CE, Shih WH, Shih WY. Analyst. 2014; 139:2754–2763. [PubMed: 24759937]

38. Zhu Q, Shih WY, Shi WH. Sensor Actuat B-Chem. 2009; 138:1–4.
39. Zhu Q, Shih WY, Shih W-H. Appl Phys Lett. 2008; 92:183505. [PubMed: 19479043]
40. Shih WY, Zhu Q, Shih WH. J Appl Phys. 2008:104.
41. Zhu Q, Shih WH, Shih WY. Sensor Actuat B-Chem. 2013; 182:9.
42. Wu W, Shih WY, Shih WH. Journal of Applied Physics. 2013:114.
43. Bazan V, Agnese V, Corsale S, Calo V, Valerio MR, Latteri MA, Vieni S, Grassi N, Cicero G, Dardanoni G, Tomasino RM, Colucci G, Gebbia N, Russo A. Ann Oncol. 2005; 16(Suppl 4):iv50–55. [PubMed: 15923430]
44. Eser S, Schnieke A, Schneider G, Saur D. Br J Cancer. 2014; 111:817–822. [PubMed: 24755884]
45. Imamura Y, Morikawa T, Liao X, Lochhead P, Kuchiba A, Yamauchi M, Qian ZR, Nishihara R, Meyerhardt JA, Haigis KM, Fuchs CS, Ogino S. Clin Cancer Res. 2012; 18:4753–4763. [PubMed: 22753589]
46. Forbes SA, Bindal N, Bamford S, Cole C, Kok CY, Beare D, Jia M, Shepherd R, Leung K, Menzies A, Teague JW, Campbell PJ, Stratton MR, Futreal PA. Nucleic Acids Res. 2011; 39:D945–950. [PubMed: 20952405]
47. Ugozzoli LA, Latorra D, Puckett R, Arar K, Hamby K. Anal Biochem. 2004; 324:143–152. [PubMed: 14654057]
48. Chou LS, Meadows C, Wittwer CT, Lyon E. Biotechniques. 2005; 39:644, 646. 648 passim. [PubMed: 16312213]
49. Johnson MP, Haupt LM, Griffiths LR. Nucleic Acids Res. 2004; 32:e55. [PubMed: 15047860]
50. Kierzek E, Ciesielska A, Pasternak K, Mathews DH, Turner DH, Kierzek R. Nucleic Acids Res. 2005; 33:5082–5093. [PubMed: 16155181]
51. Koshkin AA, Singh SK, Nielsen P, Rajwanshi VK, Kumar R, Meldgaard M, Olsen CE, Wengel J. Tetrahedron. 1998; 54:3607–3630.
52. Orum H, Jakobsen MH, Koch T, Vuust J, Borre MB. Clin Chem. 1999; 45:1898–1905. [PubMed: 10545058]
53. Simeonov A, Nikiforov TT. Nucleic Acids Res. 2002; 30:e91. [PubMed: 12202779]
54. Tolstrup N, Nielsen PS, Kolberg JG, Frankel AM, Vissing H, Kauppinen S. Nucleic Acids Res. 2003; 31:3758–3762. [PubMed: 12824412]
55. You Y, Moreira BG, Behlke MA, Owczarzy R. Nucleic Acids Res. 2006; 34:e60. [PubMed: 16670427]
56. Land MA, Webster J, Christoforou A, Praveen D, Jeffery P, Chalmers J, Smith W, Woodward M, Barzi F, Nowson C, Flood V, Neal B. BMJ open. 2014; 4:e003720.
57. MD-Health. http://www.md-health.com/Normal-Urine-Output.html, David C. Dugdale, III, MD, Professor of Medicine, Division of General Medicine, Department of Medicine, University of Washington School of Medicine. Also reviewed by David Zieve, MD, MHA, Bethanne Black, and the A.D.A.M. Editorial team
58. Kirimli CE, Shih WH, Shih WY. Analyst. 2013; 138:6117–6126. [PubMed: 23964355]
59. Soylu MC, Shih W-H, Shih WY. Industrial & Engineering Chemistry Research. 2013; 52:2590–2597.
60. Soylu, MÇ. Piezoelectric Plate Sensor for in situ Genetic Detection of Hepatitis B Virus in Serum without DNA Isolation and Amplification. 2013. Drexel University; Drexel University; 2013.

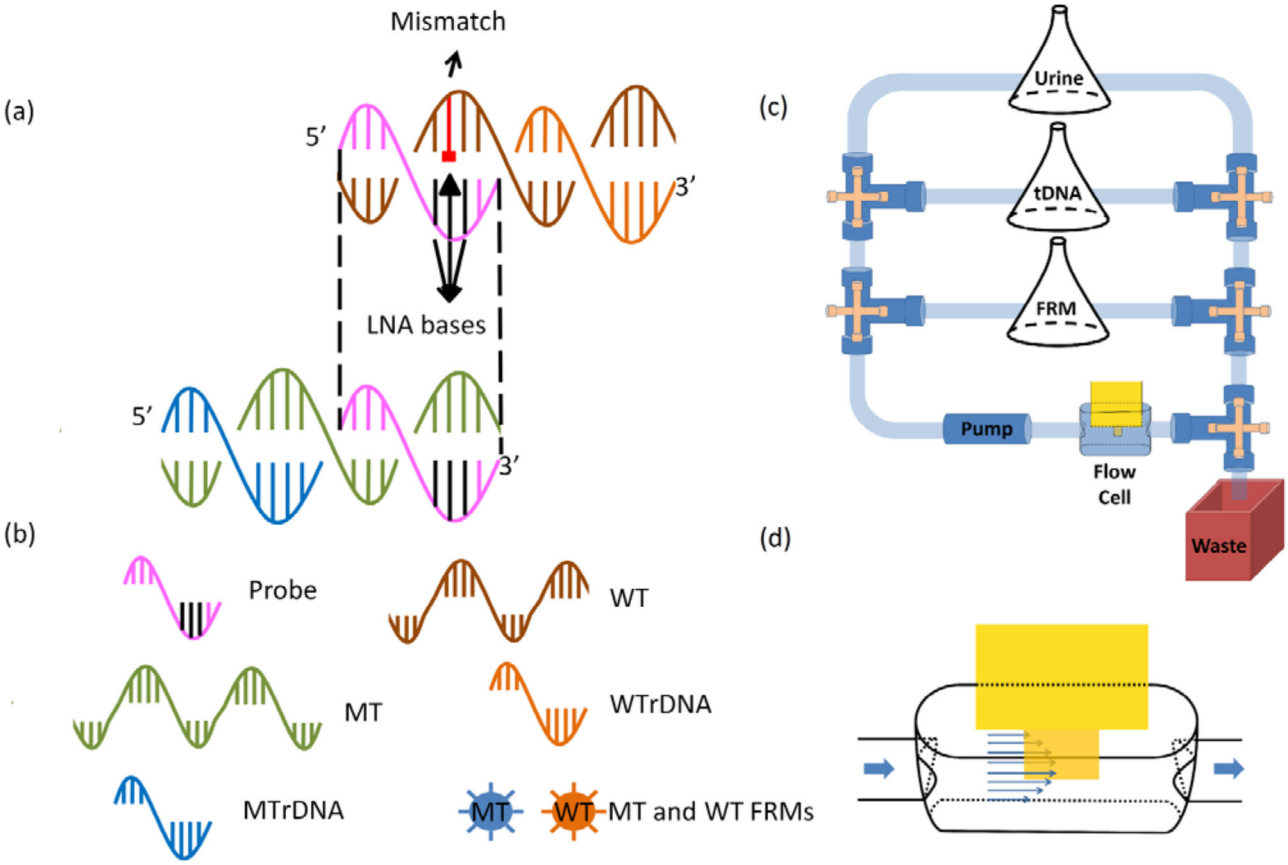

Figure 1.

(a) A schematic of the relationship between probe, mutant (MT) target DNA, wild type (WT), MT reporter DNA (MTrDNA), and WT rDNA (WTrDNA) for *KRAS* point mutation, (b) the legend for schematic in (a), (c) a schematic of the flow system for mutation detection in urine and (d) a blow-up of the PEPS situated in the center of the flow cell.

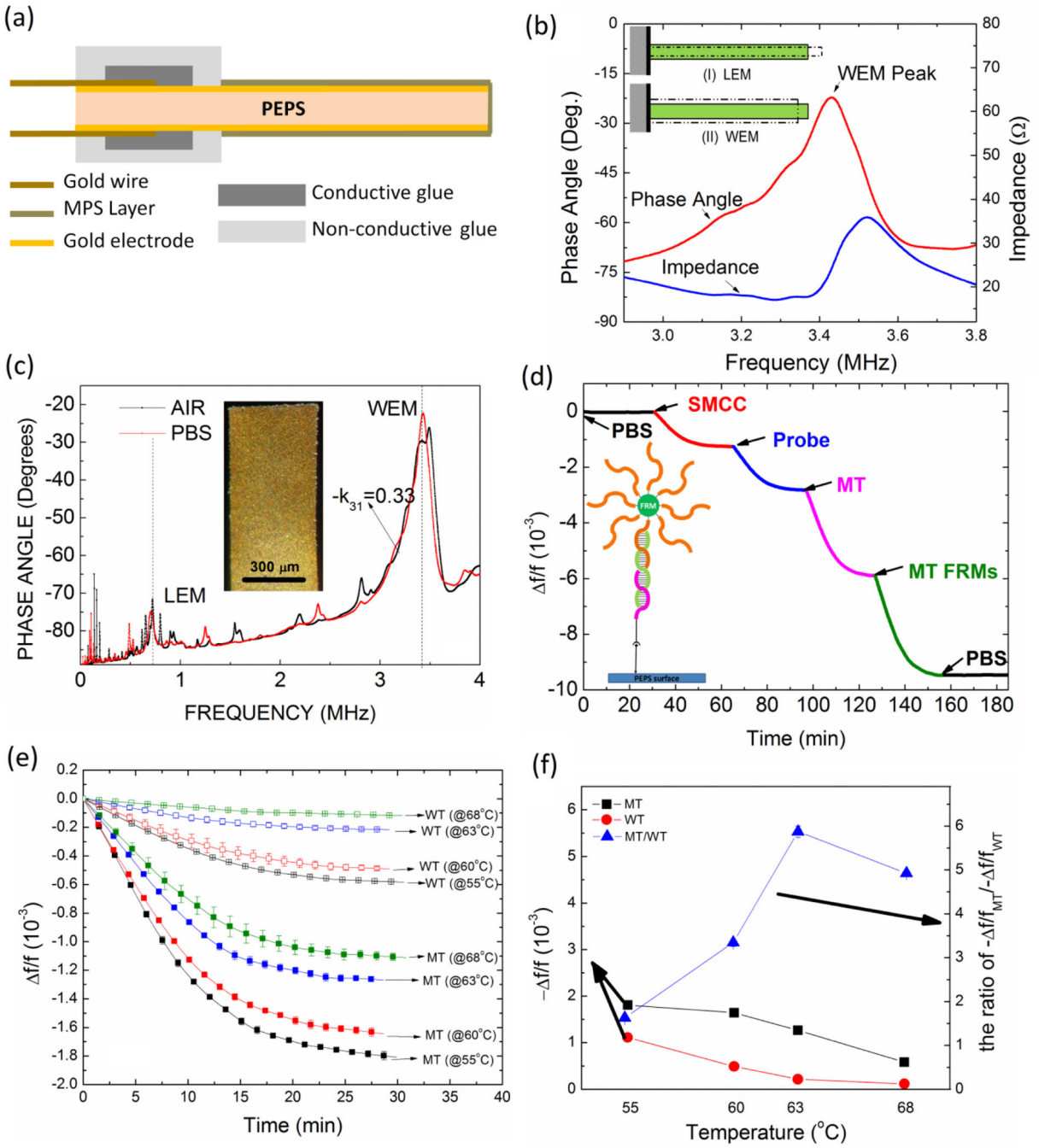

Figure 2.

(a) A schematic of the side view of the PEPS. The gold wires were connected to the top and bottom gold electrodes with conductive glue. The entire ear end including the conductive glue was covered with non-conductive glues. MPS layer covered the front end of the PEPS that was not covered by the nonconductive glue. (b) The blowup of both the impedance-versus-frequency (blue) and phase angle-versus-frequency (red) spectra around the WEM resonance peak around 3.4 MHz. Also included are schematics for LEM and WEM vibrations in insert (I) and (II), respectively. (c) In-air (black) and in-PBS (red) phase angle-

versus-frequency resonance spectra with an insert showing an optical micrograph of the PEPS, and (d) relative resonance frequency shift, Δf/f, of the PMN-PT PEPS going through PBS step (0-30 min), the SMCC bonding step (30-60 min), the probe immobilization step(60-90 min), the MT detection step (90-120 min), the MT FRMs detection step (120-150 min), and the final PBS step (150-180 min) with an insert showing a schematic of the molecules involved in these steps. (e) MT (solid symbols) and WT (open symbols) detection at 1×10^{-15} M in PBS at 55°C (black), 60°C (red), 63°C (blue) and 68°C (green) for 30 min, (f) average −Δf/f at 25-30 min versus temperature, squares for MT and circles for WT. Also plotted is the ratio of the average −Δf/f at 25-30 min of the MT to that of the WT (triangles) (the right side of the double-y plot)

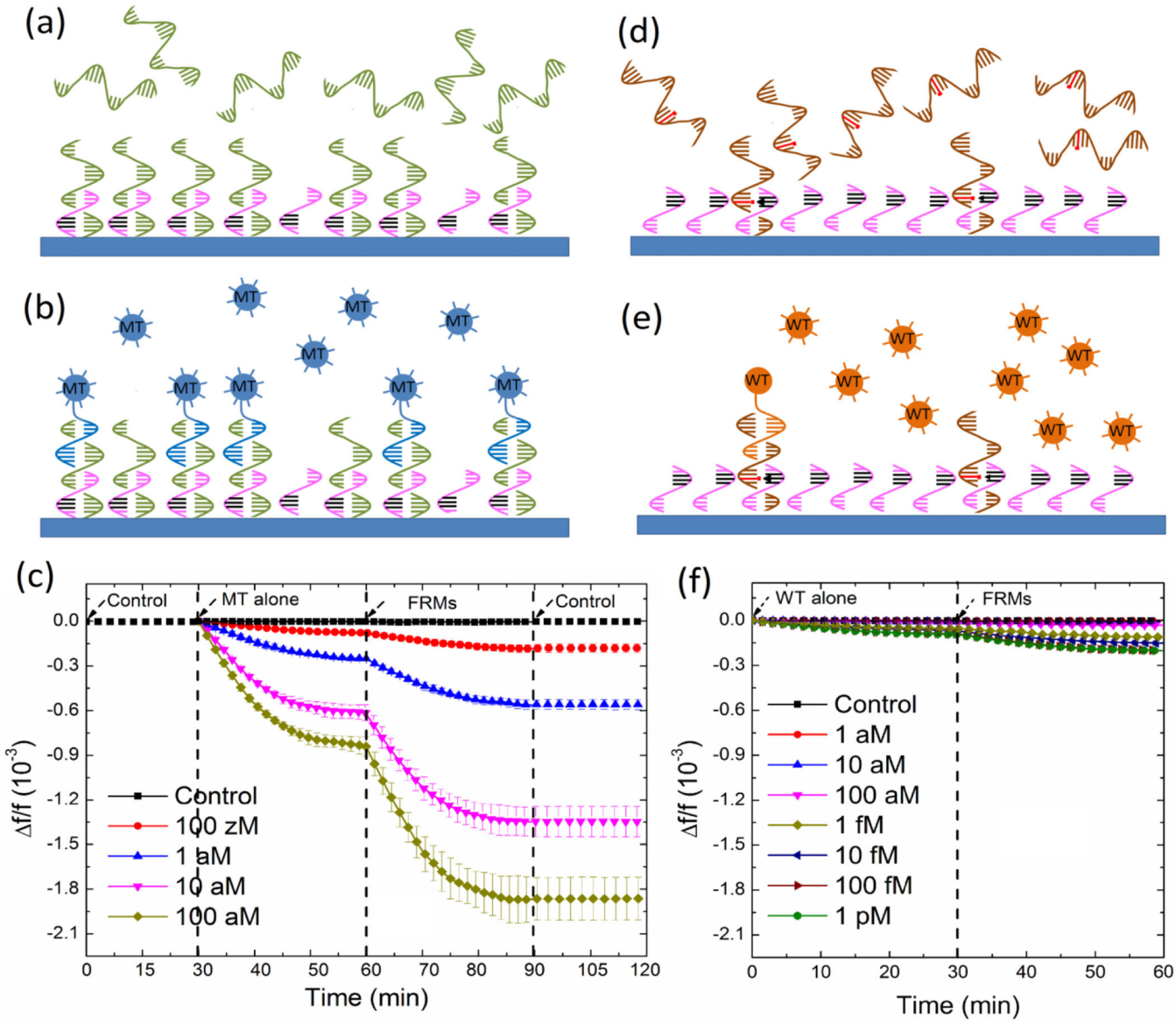

Figure 3.

A schematic representation of (a) MT detection (b) MT FRMs detection following MT detection, (c) Δf/f versus time of MT detection followed by MT FRMs detection including the background signal collection in urine before (0-30 min) and after (90-120 min) the MT and FRMs detection, (d) WT detection (e) WT FRMs detection following WT detection, (f) Δf/f versus time of WT detection followed by WT FRMs detection. Clearly, at 63°C and at a flow rate of 4 mL/min, the detection $-\Delta f/f$ of 1 aM MT at t = 30 min ($-\Delta f/f = 0.2\times10^{-3}$) was much larger than that of WT at 100 fM at t = 30 min, ($-\Delta f/f < 0.1\times10^{-3}$), indicating the specificity of the MT detection at such detection conditions.

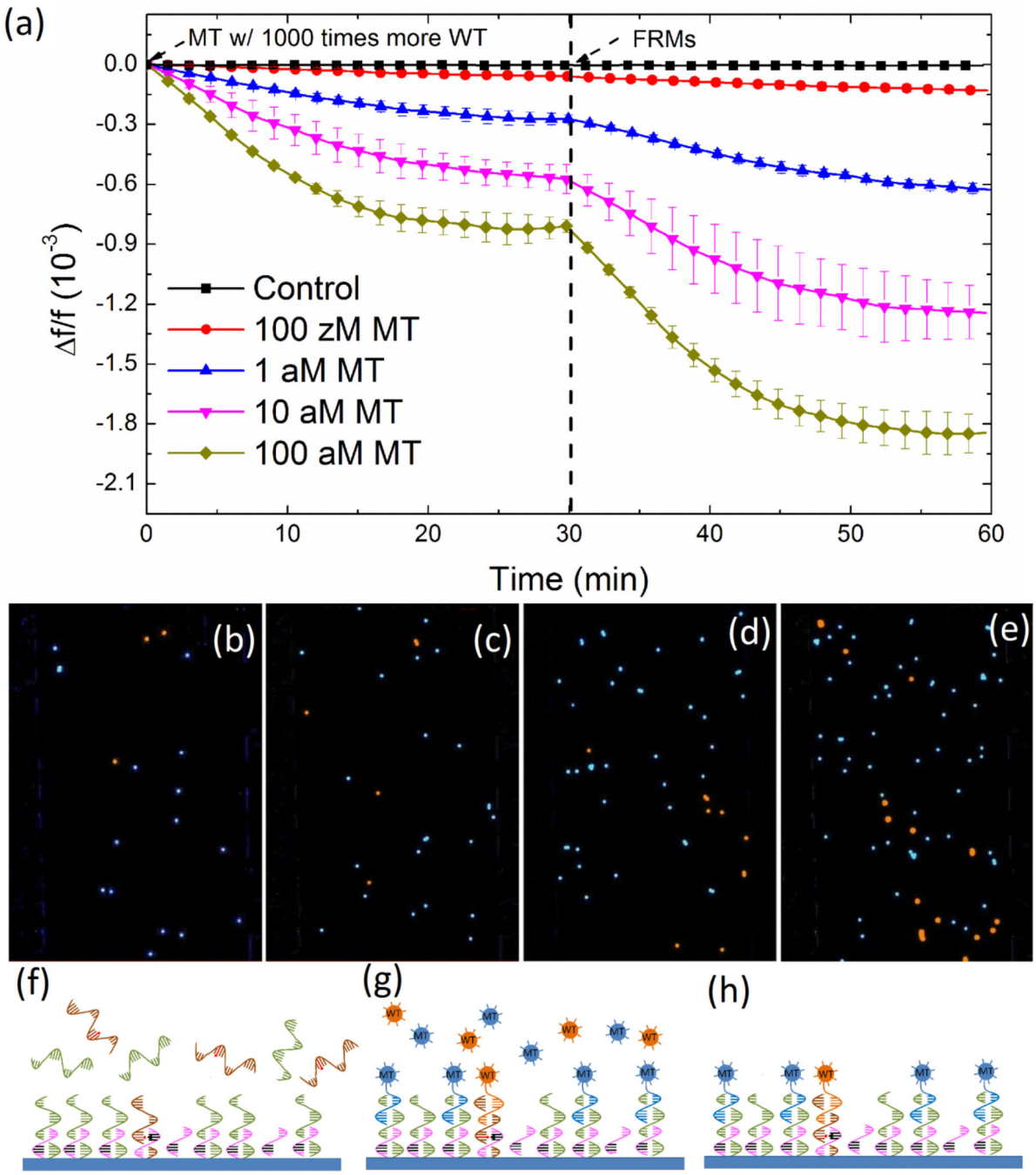

Figure 4.

(a) Relative resonance frequency shift, Δf/f versus time of PEPS detection of MT in a background of 1000-fold more WT at various MT concentrations followed by detection in an equal mixture of 10^5 FRMs/mL of MT FRMs and 10^5 FRMs/mL of WT FRMs in PBS, (b), (c), (d), and (e) are respectively the fluorescent images of the PEPS obtained after the FRMS detection following the MT detections at 0.1 aM (100 zM), 1 aM, 10 aM, and 100 aM MT concentrations where the blue color denotes the MT FRMs while the orange color denotes the WT FRMs, (f), (g), and (h) are respectively the schematic illustrating the PEPS

in a mixture of MT and WT at t=0-30 min in (a), a schematic of the PEPS in a mixture MT FRMs and WT FRM at t= 30-60 min in (a), and a schematic of the PEPS after the final washing. That there were far more MT FRMs captured than WT FRMs in (b)-(e) indicates that the detection of MT was specific even in a background of 1000 times more WT.

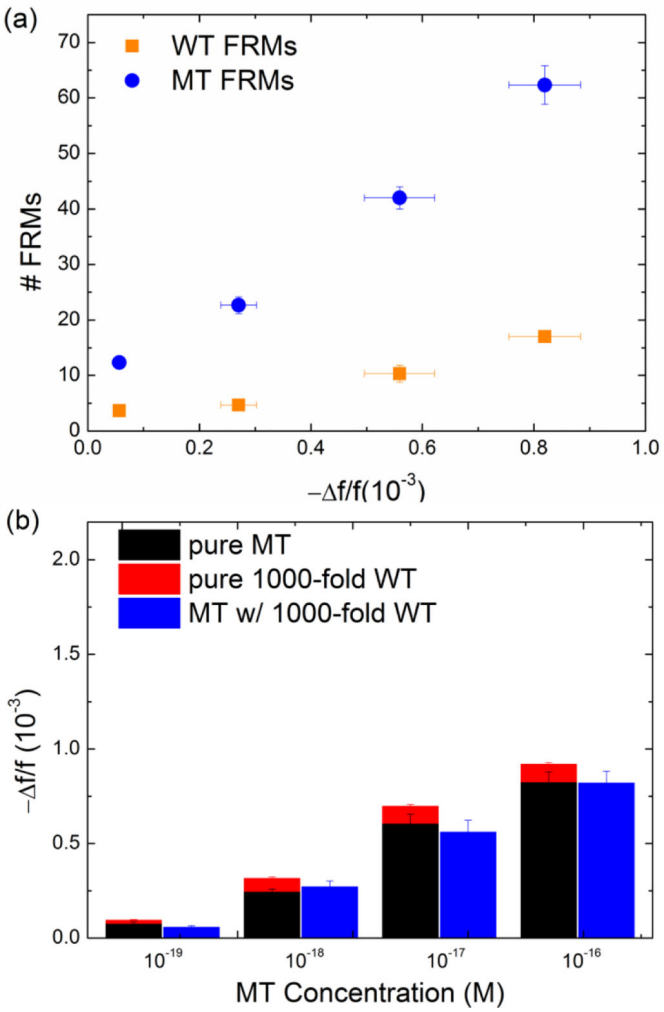

Figure 5.

(a) Number of MT FRMs (blue full circles) and that of WT FRMs (orange full squares) obtained from Figs. 5(b)-5(e) versus average PEPS MT detection −Δf/f at t = 25-30 min taken from Fig. 4(a). Note for each MT concentration the number of MT FRMs (blue) was still roughly 4 times higher than that of the WT even the concentration of the WT was 1000 times higher than that of the MT. This indicates that in each case more than 80% of the detection Δf/f was due to the binding of the MT and that PEPS's MT detection was specific even the concentration of the WT was 1000 times higher than that of the MT. (b) Comparison of −Δf/f for detection averaged over t = 25-30 min of pure MT in Fig. 4(c) (black), that at 1000-fold pure WT taken from Fig. 4(f) (red) and that in a mixture of MT in 1000-fold more WT as taken from Fig. 5(a) (blue). That the −Δf/f in a mixture of MT in 1000-fold (blue) was similar to the sum of the −Δf/f of MT and the −Δf/f of 1000-fold WT more WT indicates that the presence of the 1000-fold WT had negligible effect on the MT detection. In addition, that the −Δf/f of pure MT (black) was also roughly 4 times that of 100-fold pure WT (red), further confirming the specificity of the current PEPS single-nucleotide mutation detection.

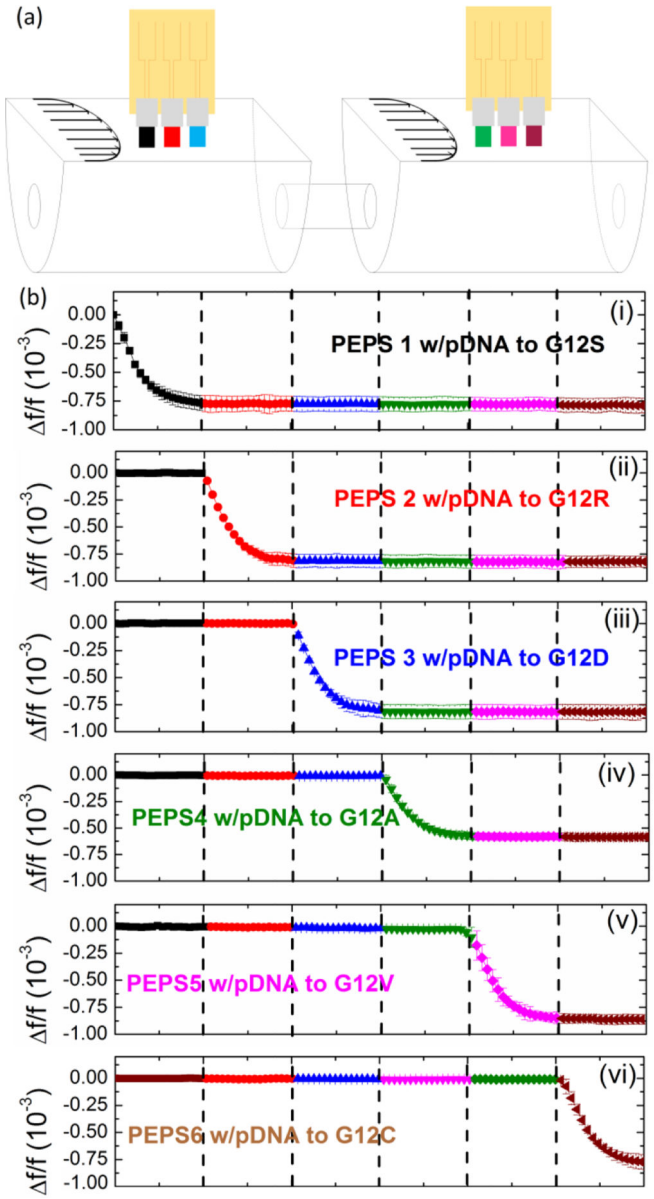

Figure 6.

(a) A schematic of a 6-PEPS array in two flow cells to detect 6 codon-12 *KRAS* mutations and (b) Relative frequency shift, PEPSs each coated with an LNA pDNA complementary to one of the 6 codon-12 *KRAS* mutations where 6 different urine samples each spiked with a different 12 *KRAS* mutation (coded with 6 different colors) were flown over the array PEPSs each for 30 min in succession.

Table I

Sequencies the probe, MT, WT, MTrDNA, and the WTrDNA and the melting temperatures (T_m) of MT with probe, WT with probe, MTrDNA with MT, and WTrDNA with WT.

Type of DNA	Sequence (5′→3′)	T_m
Probe (17 nt)	Amine-(PEG)12-TGGAGCTG**T**TGGCGTAG	---
MT (50 nt)	TCTGAATTAGCTGTATCGTCAAGGCACTCTTGCCTACGCCA**A**CAGCTCCA	70°C (Probe to MT
WT (50 nt)	CTACGCCA**C**CAGCTCCAACTACCACAAGTTTATATTCAGTCATTTTCAGC	55°C (Probe to WT)
MTrDNA (33 nt)	GCAAGAGTGCCTTGACGATACAGCTAATTCAGA-(PEG)7-Amine	78.5°C (MTrDNA to MT)
WTrDNA (33 nt)	Amine-(PEG)12-GCTGAAAATGACTGAATATAAACTTGTGGTAGT	73.6°C (WTrDNA to WT)

Note that the site where the mutation occurs is underlined in the MT, WT, and probe and the LNA bases in the probe are marked in red. The melting temperatures were estimated using a 115mM salt concentration consistent with urinary salt content[56,57] and a LNA/DNA concentration of 50 nM.

Table II

Codon-12 *KRAS* mutations, corresponding LNA probe sequences, melting temperature of the LNA probe with its corresponding MT and that with the WT, the melting temperature difference between the MT and the WT with the probe, and the PEPSs in the 6-PEPS array that target them.

Mutation	Probe	T_m of MT to probe (°C)	T_m of WT to probe (°C)	ΔT_m (°C)	
GGT→AGT (G12S)	Biotin-(PEG)12-TGGAGCT**A**GTGGCGTAG	68	52.7	15.3	PEPS1
GGT→CGT (G12R)	Biotin-(PEG)12-TGGAGCT**C**GTGGCGTAG	71	50.1	20.9	PEPS2
GGT→GAT (G12D)	Biotin-(PEG)12-TGGAGCTG**A**TGGCGTAG	70	54.7	15.3	PEPS3
GGT→GCT (G12A)	Biotin-(PEG)12-TGGAGCTG**C**TGGCGTAG	72	51.1	20.9	PEPS4
GGT→GTT (G12V)	Biotin-(PEG)12-TGGAGCTG**T**TGGCGTAG	70	54.3	15.7	PEPS5
GGT→TGT (G12C)	Biotin-(PEG)12-TGGAGCT**T**GTGGCGTAG	69	53.3	15.7	PEPS6

*Red letters indicate codon 12; Bold letters mutation sites; Underlines LNAs. The melting temperatures were estimated using a 115mM salt concentration consistent with urinary salt content[56,57] and a LNA/DNA concentration of 50 nM.